

# Load Dynamics in Piezoelectric Actuation

J.R. van Hulzen, G. Schitter, P.M.J. Van den Hof and J. van Eijk

**Abstract**—High control performance is essential in many precision positioning applications, such as control of the vertical sample position in a atomic-force microscope (AFM). This paper investigates the impact of load flexibility on piezoelectrically actuated positioning systems in terms of control performance. The modeling method used combines modal analysis with simple transfer function manipulations, and shows, how the load dynamics may influence the control performance. The analysis is experimentally verified on a commercial AFM system.

## I. INTRODUCTION

Piezoelectric actuation is often used in applications requiring high-precision positioning at high bandwidths. A typical application of such a positioning system is the atomic-force microscope (AFM) [1]. An AFM uses a very sharp tip to scan the surface topography of a sample on a nanometer scale (see [2] for an overview).

A crucial limitation in imaging speed of AFMs is the bandwidth of the vertical axis positioning system. The purpose of this system is to keep the tip-sample forces constant by tracking the sample topography. Recently, improvements to the positioning system of the vertical axis have been proposed. The mechanical design has been improved by making the scanner smaller and more rigid [3],[4] and by balancing of the vertical stage by using two counteracting actuators [5]. Model-based controllers for the lateral and vertical axis have been implemented [4],[6]-[10] and have been shown to improve performance.

The introduction of stiff and lightweight designs and the application of model-based controllers naturally leads to the question what the influence of the load dynamics is on the control performance of the system, and whether the load dynamics can be adjusted so as not to limit the control performance.

This question has also been raised in [11] where for piezo stack actuators it has been claimed that adjusting the load dynamics to the piezo dynamics (load balancing) is highly beneficial for the control performance of the system. In that work the piezo actuator has been modeled as a distributed parameter system [11], [12] assuming a rigid load.

In [13], [14] finite element analysis (FEA) has been used to derive a model of a tube scanner in unloaded and

This work is part of a project on Model-based subnano-positioning control systems for high-end professional equipment and microsystems manipulation and is sponsored by the Delft Center for Mechatronics and Microsystems and the National Institute of Health (RO1 GM 065354)

J.R. van Hulzen, G. Schitter, P.M.J. Van den Hof are with the Delft Center for Systems and Control, Delft University of Technology, Mekelweg 2, 2628 CD Delft, The Netherlands, J.R. van Hulzen, G. Schitter, J. van Eijk are with the Precision and Microsystems Engineering Department, Delft University of Technology, Mekelweg 2, 2628 CD Delft, The Netherlands, j.r.vanhulzen@tudelft.nl

loaded conditions. The FEA models can be reduced to low-order models which are well suited for control design. A disadvantage of FEA modeling is that parametric analysis of load conditions is hard to perform.

In this paper we will consider the effect of loads on tube scanners following a modeling approach that is similar to the receptance coupling method [15]-[17], where the frequency response function (FRF) of a system is obtained from the FRFs of subsystems. The model posed by [11] is used as a basis and extended to include both rigid and dynamic loads. Using the extended model, the influence of the load on control performance (in terms of control bandwidth) can be made explicit using a limited set of parameters.

This paper is organized as follows. In Section II, a dynamical model based on modal approximation is derived. Two cases are discussed, the unloaded actuator and the actuator combined with a rigid load. Next, the model is extended to include one or more non-rigid loads. In Section III, the model is used to describe the dynamics of a commercially available AFM. Two cases involving dynamic loads are investigated and the results are verified experimentally. Finally, conclusions are given in Section IV.

## II. DYNAMICS OF PIEZO ACTUATED SYSTEMS

A piezoelectric actuator consists of a stiff ceramic material which expands under the influence of an electric field. In [11] a dynamical model of a piezo actuator is proposed, where axial vibration in the piezo material is modeled using a partial differential equation.

### A. Axial vibration in unloaded tube scanner

The vertical axis of a tube scanner is modeled as an axially loaded rod with constant cross section under the assumptions that there is neither bending nor shear and that the tube retains its shape during extension. The axial displacement  $u(x, t)$  in the piezo material is modeled using a second order partial differential equation

$$EA \frac{\partial^2 u(x, t)}{\partial x^2} + f(x, t) = A\rho \frac{\partial^2 u(x, t)}{\partial t^2}; \quad 0 < x < L \quad (1)$$

in which  $L$  is the length of the material,  $E$  is the modulus of elasticity,  $A$  the area and  $\rho$  the density. The force generated by the piezoelectric effect per unit length is denoted as  $f(x, t)$ . The solution of (1), assuming  $f(x, t) = 0$ , yields the natural modes which are given in [18] for various configurations. The frequencies at which the natural modes occur are given by

$$\omega_i = \frac{\lambda_i}{L} \sqrt{\frac{E}{\rho}}, \quad i = 1, 2, 3, \dots, \infty \quad (2)$$

where  $\lambda_i$  is a series of values determined by the solutions to the eigenvalue problem associated with the boundary value problem. Unloaded, the actuator is fixed on one end and free on the other and we have the boundary conditions  $u(0, t) = 0$  and  $\partial u(L, t)/\partial x = 0$  which yield

$$\lambda_i = \frac{(2i - 1)\pi}{2}. \quad (3)$$

The steady state response of the system to a harmonic excitation in the form  $f(x, t) = F(x)e^{j\omega t}$  can be derived using modal analysis [19]. In the fixed-free configuration the net force generated by the piezoelectric effect  $F(x)$  is modeled to be zero everywhere except at the free boundary  $x = L$  where  $F(x) = F_p$ . The force  $F_p$  depends on the applied electric field [21]. The response  $u(x, t)$  to harmonic excitation  $f(L, t) = F_p e^{j\omega t}$  evaluated at the free boundary  $x = L$  is given by  $u(L, t) = P_a(\omega)F_p e^{j\omega t}$  where

$$P_a(\omega) = \sum_{i=1}^{n_m} \frac{\phi_i^2(L)}{\mu_i(\omega_i^2 - \omega^2)} + R. \quad (4)$$

The frequency response function  $P_a(\omega)$  depends on the modal mass  $\mu_i$ , residual  $R$  and mode shape  $\phi_i$  given by

$$\mu_i = \frac{\rho AL}{2}, \quad R = \frac{L}{EA} - \sum_{i=1}^{n_m} \frac{\phi_i^2(L)}{\mu_i \omega_i^2}, \quad \phi_i(L) = \sin \lambda_i. \quad (5)$$

Intrinsic damping in a piezoelectric material is hard to predict and is often determined experimentally. Assuming proportional damping [19] the model (4) is extended to

$$P_a(\omega) = \sum_{i=1}^{n_m} \frac{\phi_i^2(L)}{\mu_i(\omega_i^2 - \omega^2 + 2j\xi_i\omega_i\omega)} + R, \quad (6)$$

in which  $\xi_i$  are calculated using  $\xi_i = \frac{1}{2}(\alpha\omega_i^{-1} + \beta\omega_i)$ . By setting  $\xi_1$  and  $\xi_2$  equal to an experimental determined  $\xi$ ,  $\alpha$  and  $\beta$  can be eliminated resulting in

$$\xi_i = \frac{\omega_1\omega_2 + \omega_i^2}{\omega_i(\omega_1 + \omega_2)}\xi. \quad (7)$$

If we let the number of modes  $n_m$  in (6) tend to infinity we can write  $P_a(\omega)$  as

$$P_a(\omega) = \frac{N_a}{D_a} = k_0 \frac{\prod_{i=1}^{\infty} (z_i^2 + 2\xi_i^z z_i j\omega - \omega^2) p_i^2}{\prod_{i=1}^{\infty} (p_i^2 + 2\xi_i^p p_i j\omega - \omega^2) z_i^2}, \quad (8)$$

in which  $k_0 = L/EA$  is the static stiffness of the system. The complex conjugate poles of  $P_a(\omega)$  are the resonant modes of the system given by (2) and (3) such that  $p_i = \omega_i$ . The complex conjugate zeros of the system are the roots of  $N_a$  and can be derived by solving (1) under the assumption that  $u(L, t) = 0$  [20]. This leads to the boundary conditions corresponding to the fixed-fixed case given by  $u(0, t) = 0$ ,  $u(L, t) = 0$ . With (2) and  $\lambda_i = i\pi$  we arrive at

$$z_i = \frac{i\pi}{L} \sqrt{\frac{E}{\rho}}, \quad p_i = \frac{(2i - 1)\pi}{2L} \sqrt{\frac{E}{\rho}}, \quad i = 1, 2, \dots, \infty. \quad (9)$$

The damping factors for the poles  $\xi_i^p$  and zeros  $\xi_i^z$  in (8) are determined by substituting  $\omega_i$  by  $p_i$  and  $z_i$  in (7).

### B. Axial vibration in tube scanner loaded by a rigid mass

Suppose that the free end of the actuator is loaded by a concentrated mass  $m_l$  which is attached at  $x = L$ . In this case the boundary conditions change to

$$u(0, t) = 0, \quad -EA \frac{\partial u(L, t)}{\partial x} = m_l \frac{\partial^2 u(L, t)}{\partial t^2}$$

and the solutions of the eigenvalue problem are [18], [19]

$$\cot \lambda_i = \frac{m_l}{\rho AL} \lambda_i. \quad (10)$$

We are interested in the transfer function  $P_{al}(\omega)$  giving the relationship between harmonic excitation at  $x = L$  and displacement of the load. Because the load is rigid the displacement of the load is equal to the actuator extension  $u(x, t)$  evaluated at  $x = L$ .  $P_{al}(\omega)$  has the same structure as (4). The natural modes  $\omega_i$  are derived using (10) and (2) and the mode shapes  $\phi_i(x)$  evaluated at the interface between actuator and load are given by (10) and (5). Using the orthogonality relations [19] we have

$$\begin{aligned} \mu_i &= \rho A \int_0^L \sin^2 \lambda_i \frac{x}{L} dx + m_l \sin^2 \lambda_i \\ &= \frac{1}{2} \rho AL - \frac{1}{2} \rho AL \lambda_i^{-1} \sin \lambda_i \cos \lambda_i + m_l \sin^2 \lambda_i \end{aligned}$$

inserting  $\rho AL/\lambda_i = m_l \tan \lambda_i$  yields

$$\mu_i = \frac{1}{2} \rho AL + \frac{1}{2} m_l \sin^2 \lambda_i, \quad (11)$$

in which  $\lambda_i$  is determined using (10).

From (2), (10) and (11) it is clear that a load  $m_l$  of zero is identical to the unloaded case. In this case  $\cot \lambda_i = 0$  and thus  $\lambda_i$  is  $\frac{1}{2}\pi, \frac{3}{2}\pi, \frac{5}{2}\pi, \dots, \infty$  which is identical to (3). If the load tends to infinity  $\cot \lambda_i$  also tends to infinity and thus  $\lambda_i$  tends to  $0, \pi, 2\pi, 3\pi, \dots, \infty$ . Because the load is rigid the displacement of the load is equal to  $u(L, t)$  and we can determine the zeros of the transfer function using the same boundary conditions as used in the unloaded case [20]. This result also implies that the zeros of the transfer function are unaffected by the size of a rigid load. Thus, using (10) we conclude that an increasing load shifts the poles of  $P_a(\omega)$  towards the zeros. The exception to this rule is the pole-pair corresponding to the first mode which shifts towards the origin. In Fig. 1 the influence of a rigid mass on a piezo actuator is shown. The actuator dynamics are determined using  $E = 55 \text{ GPa}$ ,  $\rho = 7.8 \times 10^3 \text{ kg/m}^3$ ,  $L = 45 \text{ mm}$  and  $\xi = 0.0066$ . The transfer function is scaled by the static actuator stiffness  $k_0 = EA/L$ .

The influence of the load on the peak gain of a mode depends on the damping of the mode. In Fig. 2 the peak gain of the second mode (Fig. 1) is shown for damping values  $\xi$  ranging from 0.0033 to 0.015. Loads smaller than 10% of the actuator mass are negligible. Loads equal to the actuator mass show a decrease in peak gain of about 12 dB. Above this an increase of the load by a factor of two results in a decrease of the peak gain of 6 dB. For loads above 30 times the actuator mass the poles are effectively canceled.

From Fig. 1 it is clear that from a control design perspective a rigid load has a number of advantages. Because the

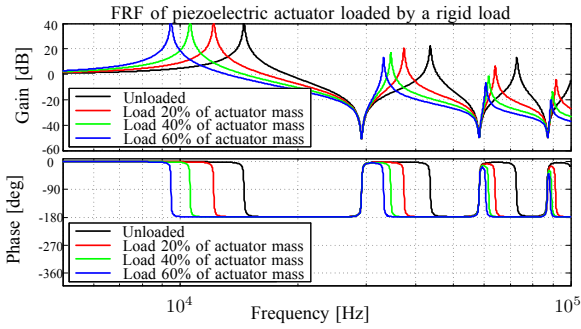


Fig. 1. FRF of an unloaded piezo actuator (black) and a piezo actuator loaded by a rigid mass equal of 20% (red), 40% (green) and 60% (blue) of the actuator mass.

load is rigid, the poles of the transfer function can not be shifted to lower frequencies than the zeros. This implies that the phase lag introduced by the mechanical system does not exceed 180 degrees. A second advantage is that the peak gain of the second and higher modes is reduced due to the proximity of the zeros. This is achieved by balancing forces rather than by introducing damping. This has the advantage that no additional noise is introduced in the control loop which benefits precision positioning. Furthermore, a rigid load shifts all modes, so also the peak gain of modes above the controller bandwidth is reduced. The result is that disturbances caused by excitation of modes outside the controller bandwidth (spill over) are reduced. A clear disadvantage of a heavy load is that the first mode shifts to a lower frequency and that more energy is required to achieve the same displacement.

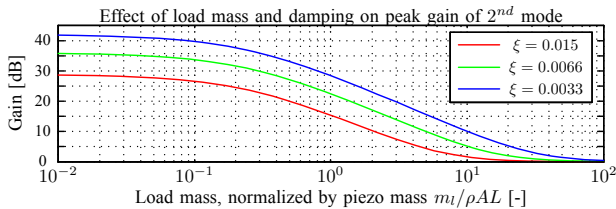


Fig. 2. Reduction in peak gain of second mode due to rigid load.

### C. Axial vibration in tube scanner loaded by a flexible mass

In most practical applications the load is flexible rather than rigid. The resonant modes of the load should be taken into account by extending (6). If the resonant modes of the load are in the same frequency range as the low order modes of the actuator a simple representation of the load is often sufficient to capture the impact of load flexibility on control design. In this case, the load can be modeled as a discrete fourth order system with two rigid masses connected by a spring. More complex load cases can be modeled by connecting two or more of these systems, either in series or in parallel. In Fig. 3 and Fig. 6 a piezoelectric actuator loaded by one or more flexible loads is shown. Loads are labeled as  $q = 1, 2, \dots$  and have identical frequency response

functions  $P_{lq}$  defined as

$$P_{lq} = \frac{x_{q1}}{F_q} = \frac{k_q - m_{q2}\omega^2}{-\omega^2(k_q(m_{q1} + m_{q2}) - m_{q1}m_{q2}\omega^2)},$$

which can be rewritten to  $P_{lq} = N_{lq}D_{lq}^{-1}$  with

$$N_{lq} = \frac{z_q^2 - \omega^2}{z_q^2}, \quad D_{lq} = -m_{tq}\omega^2 \frac{p_q^2 - \omega^2}{p_q^2},$$

in which we have  $m_{tq} = m_{q1} + m_{q2}$  and

$$z_q = \sqrt{\frac{k_q}{m_{q2}}}, \quad p_q = \sqrt{\frac{k_q}{m_{q1}} + \frac{k_q}{m_{q2}}}.$$

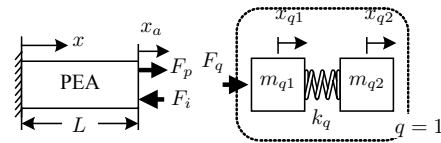


Fig. 3. The piezoelectric actuator loaded by a single non-rigid mass.

1) *Case 1, Single flexible load:* The transfer function of the loaded actuator can be derived using the free body diagram shown in Fig. 3. We have  $x_a = P_a(F_p - F_i)$  and  $x_{11} = P_{l1}F_1$  in which  $F_i = F_1$  represents the force balance between actuator and load. Because the load is connected to the actuator at all times we have  $x_a = x_{11}$  and

$$P_{x_{11}} = \frac{x_{11}}{F_p} = \frac{P_a P_{l1}}{P_a + P_{l1}},$$

which can be rewritten as

$$P_{x_{11}} = \frac{x_{11}}{F_p} = \frac{N_a N_{l1}}{D_a N_{l1} + D_{l1} N_a}, \quad (12)$$

and because  $x_{12} = N_{l1}^{-1}x_{11}$  it follows that

$$P_{x_{12}} = \frac{x_{12}}{F_p} = \frac{N_a}{D_a N_{l1} + D_{l1} N_a}. \quad (13)$$

To verify the accuracy of the simplified model we will derive an exact model of a piezoelectric actuator loaded by a flexible mass and compare it to (13). To simplify the analysis we assume that the load has the same cross section and material properties as the actuator. This allows the use of (4) with the length  $L$  extended by the length of the load  $L_l$ . The mode shape term  $\phi^2(L)$  is changed to  $\phi(L)\phi(L + L_l)$  to take into account that the actuator has length  $L$  and that the displacement  $u(x, t)$  is evaluated at  $x = L + L_l$ . The exact transfer function of the loaded piezoelectric actuator is then given by

$$P(\omega) = \sum_{i=1}^{\infty} \frac{\phi_i(L)\phi_i(L + L_l)}{\mu_i(\omega_i^2 + 2j\xi_i\omega_i\omega - \omega^2)}$$

in which the mode shapes  $\phi_i$  and the modal mass  $\mu_i$  are

$$\phi_i(x) = \sin\left(\frac{(2i-1)\pi}{2} \frac{x}{L + L_l}\right), \quad \mu_i = \frac{\rho A(L + L_l)}{2}.$$

The parameters for the approximate model of the load are  $m_{t1}$  and  $z_1, p_1$  which are the first eigenvalues of the fixed-free and free-free configuration. With (2) we get

$$m_{t1} = \rho AL_l, \quad z_1 = \frac{\pi}{2L_l} \sqrt{\frac{E}{\rho}}, \quad p_1 = \frac{\pi}{L_l} \sqrt{\frac{E}{\rho}}. \quad (14)$$

Fig. 4 shows a good match at low frequencies and an increasing error at high frequencies. This can be improved by including higher order modes in the model of the load.

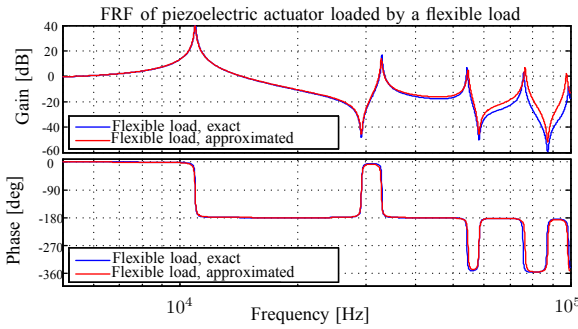


Fig. 4. Dynamics of piezo actuator loaded by a flexible load. The model is compared to the exact solution.

To determine the effect of a flexible load on the control performance we evaluate the transfer function of the loaded system using (14). By increasing the length of the load  $L_l$  from 20% to 60 % of the length of the actuator we increase the mass of the load from 20% to 60% of the actuator mass, again under the assumption that the material properties and the cross section of actuator and load are the same. From Fig. 5 it is clear that the effect of a flexible load on system performance is quite different from the rigid load case shown in Fig. 1. The flexible modes shift past the zeros which causes phase lag in excess of 180 degrees. This is a serious problem if high bandwidth control is desired since a phase lead is required over a wide frequency range. This leads to a high controller gain which in turn leads to an increased noise sensitivity. Furthermore, the advantage that the peak gain is reduced is lost if the mode shifts away from the zero.

We can conclude that the introduction of flexible loads may render the application of high bandwidth control unfeasible if the poles of the low order modes shift past a zero. However, using (13) it is possible to estimate at the system design stage whether the introduction of flexible loads such as sample disks is permissible without re-tuning the control system to a lower bandwidth.

2) *Case II, Double flexible load:* In some cases, the dynamics of the load are too complex to be captured by a single 4<sup>th</sup> order system. In these cases, the model of the load can be extended by connecting additional loads to the system. This can be done in series with the first load or parallel to it. In both cases additional poles and zeros are added to the transfer function. A series connection of loads can be treated as a single flexible load with multiple modes. The dynamics of parallel connection of two loads can be derived using the free body diagram shown in Fig. 6. From Fig. 6 we see that

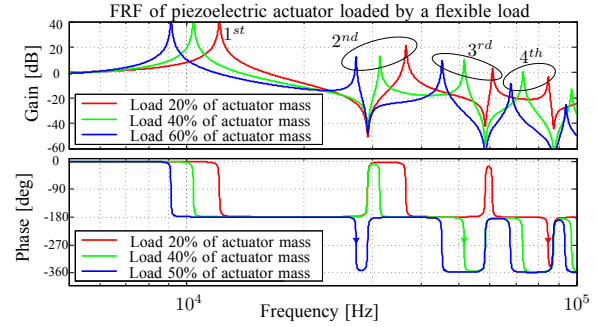


Fig. 5. Dynamics of piezo actuator loaded by a flexible load with mass equal to 20% (red), 40% (green) and 60% (blue) of the actuator mass. The material properties and cross section of actuator and load are identical.

$x_a = P_a(F_p - F_i), x_{11} = P_{l1}F_1$  and  $x_{21} = P_{l2}F_2$ . Again we find the transfer function of the interconnected system using the force balance between actuator and load  $F_i = F_1 + F_2$  and the condition  $x_a = x_{11} = x_{21}$ . It follows that

$$P_{x_{11}} = \frac{x_{11}}{F_p} = \frac{x_{21}}{F_p} = \frac{P_a(P_{l1} + P_{l2})}{P_a + P_{l1} + P_{l2}},$$

in which  $P_{l2}$  is the transfer function of the second load. With  $x_{12} = N_{l1}^{-1}x_{11}$  and  $x_{22} = N_{l2}^{-1}x_{21}$  it follows that

$$P_{x_{12}} = \frac{x_{12}}{F_p} = \frac{N_a N_{l2}}{D_a N_{l1} + D_{l1} N_a + D_{l2} N_a N_{l1}}, \quad (15)$$

and

$$P_{x_{22}} = \frac{x_{22}}{F_p} = \frac{N_a N_{l1}}{D_a N_{l1} + D_{l1} N_a + D_{l2} N_a N_{l1}}. \quad (16)$$

From (13) and (15) it is clear that an unobserved flexible load in a parallel connection with an observed flexible load simply adds a complex pair of zeros to the transfer function. The zeros associated with the actuator are unaffected. In contrast, the poles of the actuator do shift due to the presence of the second load.

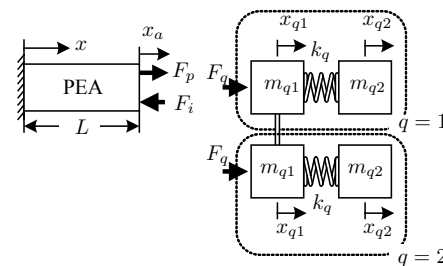


Fig. 6. The piezoelectric actuator loaded by a double non-rigid mass.

As can be concluded from the load case shown in Fig. 5, the link between the end of the actuator and the mass  $m_{12}$  should be as rigid as possible. In the case shown in Fig. 6, where two loads are connected at the end of the actuator, this link is unaffected by the presence of the second load. This effect can be exploited to improve the achievable control performance in terms of bandwidth as is shown in an example in the next section.

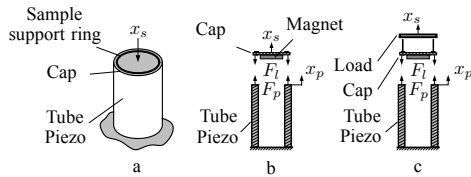


Fig. 7. Overview of tube scanner (a) with a cutout of the system (b) and the system with a sample disk as load (c).

### III. EXPERIMENTAL VERIFICATION

To study the effect of a flexible load on a piezoelectric actuator, the transfer function of the vertical axis of a piezoelectric tube scanner AFM (E-scanner, Veeco, Santa Barbara, USA) was determined using two load conditions. The layout of scanner and load conditions are shown in Fig. 7a. The system features a piezoelectric tube scanner which is fixed on one side and sealed at the free end by a thin cap. On the inside of the cap there is a magnet which holds the sample disks in place. On top of the cap there is a small ring shaped ridge which supports the sample disks. There are two load conditions of interest. The first corresponds to the single flexible load case (Fig. 7b), which is just the scanner without disk. The second corresponds to a scanner loaded by a sample disk and consists of two flexible loads connected in parallel (Fig. 7c).

The actuator extension is measured at the centerline of the tube which means that the dynamic behavior of the load is determined by the cap-magnet in combination with the sample disk. In [18] the dynamical behavior of a disk is listed for various boundary conditions. Unfortunately the boundary conditions are difficult to ascertain. The material properties and thickness of cap and magnet are unknown as well as the influence of the magnet on the sample disk. Because of this the parameters  $z_1$ ,  $p_1$  and  $m_t$  will be identified from measurements.

#### A. Case I, Single flexible load

To investigate the first load case we determine the FRF of the system using a laser vibrometer (OFV-5000 with OFV-511 sensor and VD-02 decoder, Polytec, Waldbronn, Germany) which is pointed at the center line of the tube,  $x_s$  in Fig. 7b. The load mass is increased by adding an additional magnet to the center of the cap. This corresponds to increasing  $m_{12}$  in Fig. 3. The lower two graphs of Fig. 8 show the measurement result for this load case. In the case shown in blue the load consists of the cap with the magnet inside. The measured modes are within 10% of the modes calculated using (9) with  $E = 55 \text{ GPa}$ ,  $\rho = 7.8 \times 10^3 \text{ kg/m}^3$  and  $L = 45 \text{ mm}$ . The parameters of the load model are identified as  $z_1 = 2\pi \cdot 26.5 \text{ kHz}$ ,  $p_1 = 2\pi \cdot 40 \text{ kHz}$  and  $m_t = 0.1 \text{ g}$ . If a small magnet (.9 g) is added to the center of the cap we have the load case shown in red in Fig. 8. Again the parameters of the load model are identified. The results are  $z_1 = 2\pi \cdot 21.5 \text{ kHz}$ ,  $p_1 = 2\pi \cdot 30 \text{ kHz}$  and  $m_t = 1 \text{ g}$ . From Fig. 8 it is clear that the second

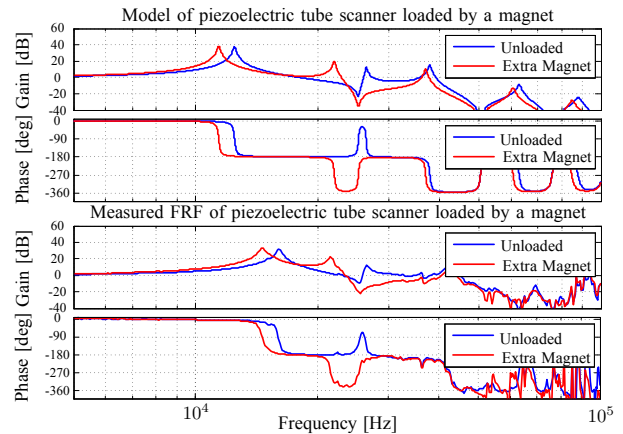


Fig. 8. Model and measurement of the AFM without additional load (blue) and the simple load case where an addition magnet is used to increase the mass of the load (red).

resonant mode shifts to a lower frequency than the first anti-resonance. The experimental results confirm the analytical results shown in Fig. 1. It is clear that the introduction of the load decreases the frequency where the phase lag exceeds 180 degrees for the first time. This is caused by the fact that pole-pair associated with the second mode shifts to a lower frequency than the first anti-resonance. The anti-resonances are unaffected by the introduction of the load.

#### B. Case II, Double flexible load

In the second load case we have the combination of the cap-magnet and one or more steel sample disks. The sample disks are supported by a ridge with radius of 9 mm. Each disk has radius of 7.5 mm, a thickness of 0.73 mm and represents a load of 1 g.

In Fig. 9, the 'unloaded' case without disks, shown in blue, is compared to a load of a single disk. The parameters found for a scanner loaded by the sample disk are  $z_1 = 2\pi \cdot 16 \text{ kHz}$ ,  $p_1 = 2\pi \cdot 30 \text{ kHz}$  and  $m_{t1} = 2 \text{ g}$  for the first 4th order system ( $q = 1$ ). For the second 4th order system ( $q = 2$ ) we have  $z_2 = 2\pi \cdot 32 \text{ kHz}$ ,  $p_2 = 2\pi \cdot 48 \text{ kHz}$  and  $m_{t2} = 1 \text{ g}$ .

Note that the identified parameters for the second load ( $q = 2$ ) are different from the parameters found in the previous section. Nevertheless, both models predict the effect of the introduction of an additional load accurately. A better match between model and measurements may be found by extending the models of load and actuator. This is not pursued here to preserve the simplicity of the analysis.

From Fig. 9 we conclude that the addition of one disk introduces a zero-pole pair between the first resonance and anti-resonance of the actuator. The introduction of additional sample disks yields the results shown in Fig. 10. The zero-pole pair between the first resonance and anti-resonance is not affected by the change in load condition. The reason for this is that the original load is connected in parallel to the introduced load.

Comparing the experimental results shown in Figs. 8, 9 and 10 and the analytical result shown in Fig. 5, it is clear that the dynamics of the load have a large influence on the

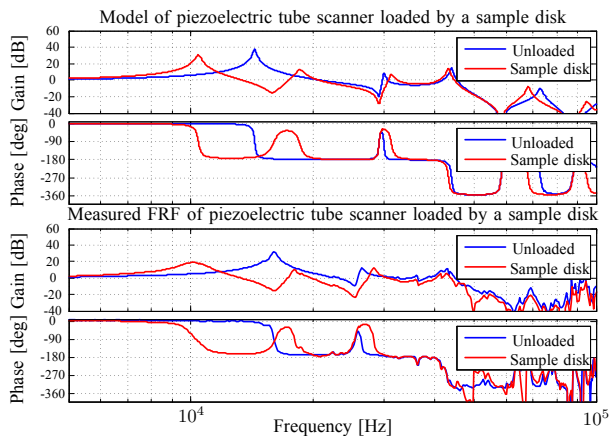


Fig. 9. Model and measurement of a the unloaded AFM (blue) and the load case where a steel sample disk is placed on the AFM (red).

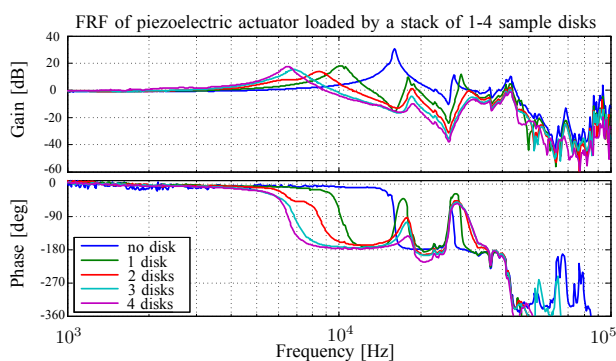


Fig. 10. FRF of an AFM loaded by 1-4 steel sample disks of 1 gr each. The FRF is scaled and corrected for phase lag introduced by the laser-vibrometer.

transfer function of the overall system. This fact may provide an additional degree of freedom in the design of control systems for flexible structures such as tube scanner AFMs.

#### IV. CONCLUSIONS

In this paper it is shown that, in piezoelectrically actuated systems, a rigid load can be used to decrease the influence of the second and higher order resonant modes of the actuator. This fact can be exploited to improve the performance of the controlled system because the peaks in the transfer function associated with these modes are reduced by counter-acting forces rather than the introduction of damping.

Unfortunately, due to the high stiffness of piezoelectric material, the resonant modes of attached loads are likely to be in the same frequency range as the modes of the actuator itself. Therefore the dynamics of the load must be taken into account in the model of the overall system.

Furthermore, because in AFM systems the measurement of the vertical position of the sample surface is used for imaging as well as feedback control, the link between actuation and sensing is likely to be flexible rather than rigid. If this is the case, the dynamics of the load causes the phase lag of

the mechanical system to exceed 180 degrees. The lowest frequency where this occurs can be considered a fundamental limit to the achievable bandwidth using feedback control.

A tube scanner AFM is an example of a system where this effect is likely to occur. In these systems the sample carrier is usually isolated from the piezo using a thin cap and held in place magnetically. Using the results obtained in section II, the design and arrangement of magnet, cap and sample carrier may be tuned to avoid a gain peak combined with a phase lag exceeding 180 degrees close to the first mode.

#### REFERENCES

- [1] G. Binnig, C.F. Quate and C. Gerber, Atomic force microscope, *Phys. Rev. Lett* 56(9), pp. 930-933, 1986.
- [2] D.Y. Abramovitch, S.B. Andersson, L.Y. Pao and G. Schitter, A Tutorial on the mechanisms, dynamics, and control of atomic force microscopes, *Proc. Amer. Ctrl. Conf.*, July 2007.
- [3] J.H. Kindt, G.E. Fantner, J.A. Cutroni and P.K. Hansma, Rigid design of fast scanning probe microscopes using finite element analysis, *Ultramicroscopy*, 100, pp. 259-265, 2004
- [4] G. Schitter, K.J. Åström, B.E. DeMartini, P.J. Thurner, K.L. Turner and P.K. Hansma, Design and modeling of a high-speed AFM-scanner, *IEEE Trans. Control Syst. Technol.*, 15(5), pp. 906-915, 2007.
- [5] T. Ando, N. Kodera, E. Takai, D. Maruyama, K. Saito and A. Toda, A high-speed atomic force microscope for studying biological macromolecules, *Proc. Natl. Acad. Sci. U. S. A.*, 98(22), pp 12468-72, 2001
- [6] S. Salapaka, A. Sebastian, J. P. Cleveland and M. V. Salapaka, High bandwidth nano-positioner: a robust control approach, *Rev. Sci. Instrum.*, 73, pp. 3232, 2002
- [7] N. Kodera, M. Sakashita and T. Ando, Dynamic proportional-integral-differential controller for high-speed atomic force microscopy, *Rev. Sci. Instrum.*, 77, pp. 083704, 2006.
- [8] D.Y. Abramovitch, S. Hoen and R. Workman, Semi-automatic tuning of PID gains for atomic force microscopes, *Amer. Ctrl. Conf.*, 2008
- [9] A.J. Fleming and S.O.R. Moheimani, Sensorless vibration suppression and scan compensation for piezoelectric tube nanopositioners, *IEEE Trans. Control Syst. Technol.*, 14(1), 2006.
- [10] G. Schitter, F. Allgöwer and A. Stemmer, A new control strategy for high-speed atomic force microscopy, *Nanotechnology*, 15, pp 108114, 2004
- [11] H. J. M. T. A. Adriaens, W. L. de Koning and R. Banning, Modeling piezoelectric actuators, *IEEE/ASME Trans. Mechatron.*, 5(4), pp. 331-341, 2000.
- [12] T. Ohara and k. Youcef-Toumi, Dynamics and control of piezotube actuators for subnanometerprecision applications, *Proc. Amer. Ctrl. Conf.*, 5, pp. 3808-3812, 1995.
- [13] J. Maess, A.J. Fleming and F. Allgöwer, Simulation of piezoelectric tube actuators by reduced finite element models for controller design, *Proc. Amer. Ctrl. Conf.*, 2007, pp.4221-4226, July 2007.
- [14] J. Maess, A.J. Fleming, F. Allgöwer, Simulation of dynamics-coupling in piezoelectric tube scanners by reduced order finite element analysis, *Rev. Sci. Instrum.*, 79, 2008
- [15] W.C. Hurty, Dynamic analysis of structural systems using component modes, *AIAA J.* 3(4), pp. 678-658, 1965
- [16] S.N. Hou, Review of modal synthesis techniques and a new approach, *Shock and Vib. Bul.*, 1969
- [17] Y. Ren, C.F. Beards, On substructure synthesis with FRF data, *J. of Sound and Vib.*, 185(5), pp. 845-866, 1995.
- [18] Blevins, R, *Formulas for Natural Frequency and Mode Shape*, Krieger Publishing Company, 2001, ISBN 1-5724-184-6.
- [19] Meirovitch L, *Fundamentals of Vibrations*, McGraw-Hill 2001.
- [20] Miu, D. K, Physical interpretation of transfer function zeros for simple control systems with mechanical flexibilities, *J. of Dyn. Syst., Meas., and Contr.*, 113(3), pp. 419-424, 1991.
- [21] An American National Standard: IEEE Standard on Piezoelectricity, ANSI/IEEE Standard 176-1987,1987